REVIEW PAPER

MODELLING ASPECTS OF SPRINKLER SPRAY DYNAMICS IN FIRES

A. W. MARSHALL and M. DI MARZO*

Department of Fire Protection Engineering, University of Maryland, College Park, MD, USA

S prinklers are used extensively in a variety of fire protection applications. These systems are required to perform effectively over a wide range of extremely harsh and complex operating conditions. The sprinkler performance depends on the initiation, formation, dispersion and surface cooling characteristics of the sprays created by these devices. The behaviour of sprinkler sprays is strongly coupled with the fire dynamics in the surrounding environment, making characterization of these sprays and their corresponding performance quite challenging. The present paper provides a discussion of the important fundamental transport process for sprinkler sprays in fires. Mathematical models are provided for these processes in order to quantitatively characterize sprinkler spray performance. These mathematical models are well suited for incorporation into CFD codes or other fire modelling tools in order to analyze and predict fire suppression performance.

Keywords: fire; suppression; spray; sprinkler.

INTRODUCTION

Sprinklers are used nearly universally in building fire protection systems. The simplicity and effectiveness of these devices have made them a popular fire suppression choice for many years. The elementary suppression mechanisms for water based suppression are *extraction of heat* from the fire gases during droplet vapourization, *displacement of oxygen* resulting from displacement of air during drop vapourization and expansion, *attenuation of heat* feedback from the fire by absorption and to a lesser extent scattering of the thermal radiation by the spray, and *surface cooling* by water vapourization on wet objects. These basic mechanisms are clearly understood; however, detailed physical models to describe and predict their behaviour are only now emerging, largely due to the complex transport behaviour at spray initiation and surface termination.

In fire research, suppression system design, and even fire investigation, it is often of interest to explore if and how these fires can be suppressed. Developments in CFD modelling have made it possible to simulate the gas (or continuous phase) behaviour of fires with a high degree of fidelity. However, before these tools can be used for fire suppression analysis, the detailed physics involved in sprinkler activa-

tion, atomization, spray dispersion and surface cooling (by drops) must be clearly understood. It is only then that descriptive models for the spray (dispersed phase) can be implemented into the CFD code. The strong coupling between the continuous phase and the dispersed phase, evidenced by the very existence of suppression, makes accurate dispersed phase models essential for fire protection analysis. The current paper characterizes sprinkler spray behaviour in a fire and presents mathematical models describing the important physical processes for sprinkler fire suppression.

The interaction between the fire and the spray has remained the central focus of research to predict and characterize sprinkler spray dispersion. Both Novozhilov (2001) and Grant *et al.* (2000) provide a thorough description of the fire–spray interaction and the resulting suppression. It should be noted that this interaction is readily predicted in CFD codes using well-developed mathematical models, which are briefly discussed herein, provided that the activation time, corresponding fire environment and initial drop characteristics are known. However, models to predict activation time and initial drop characteristics are just now emerging, making dispersion predictions challenging. The models to describe the droplet–surface interaction are also important, and the process is often neglected when modelling sprinklered fires. A discussion of these critical, yet largely unexplored, considerations is highlighted in this paper.

Correspondence to: Dr M. di Marzo, Department of Fire Protection Engineering, University of Maryland, College Park, MD 20742, USA.
E-mail: marino@eng.umd.edu

SPRINKLER ACTIVATION

Primary Sprinkler

The first sprinkler that activates as the hot gases from the fire plume flow over it is identified as the primary sprinkler. The activation time of this sprinkler is well characterized in the literature and in the fire protection engineering practice (Heskestad and Bill, 1988). The predictive model is based on a simple lumped-capacity heat transient analysis considering the heat stored in the sprinkler activation link and the convective heat transfer from the hot gases to the link itself. As the link reaches the activation temperature it collapses, opening the discharge nozzle and activating the water flow.

A parameter identified as the response time index (RTI) is introduced to group the physical characteristics of the sprinkler link. Making use of the RTI, the activation time is evaluated as:

$$t_A = \frac{RTI}{\sqrt{U}} \ln\left(\frac{T_G - T_0}{T_G - T_A}\right) \tag{1}$$

Note that the ratio of the RTI and of the square root of the gas velocity represents the time constant of the system. Further, the RTI is considered constant for a given sprinkler over a broad range of conditions. Nonetheless, some variations in the RTI are observed with the orientation of the sprinkler with respect to the gas flow. In particular, when the orientation is such that both arms and the link are exposed simultaneously to the flow, the values of the RTI are lower than for the orientation where one arm is first followed by the sprinkler link and the second arm. This second arrangement is characterized as parallel to the flow.

Secondary Sprinklers

Once the primary sprinkler is active, water is introduced in the gaseous stream in the form of droplets. The details of the spray formation will be addressed in the following. Suffice to say that large droplets will travel downward in the fire plume while smaller ones will be lifted by the updraft and may reach to the location of neighbouring (secondary) sprinklers. Finer droplets will evaporate as they follow the hot gases. Some droplets of intermediate sizes will reach the surface of the secondary sprinkler links and deposit on them. The previous analysis for the primary sprinkler is modified to reflect the evaporative cooling contribution introduced by these water droplets. The droplet volumetric fraction is introduced to relate the water volumetric flow to the air volumetric flow rate. The collection efficiency represents the fraction of those water droplets that impact the link. The estimated value of the collection efficiency is 97% of the droplets that flow through the sprinkler link cross-sectional area (Aihara and Fu, 1986). The evaporative cooling term is then given as the product of the air flow rate, the volumetric fraction of the water, its density, the collection coefficient and the latent heat of vapourization of the water. To simplify the notation, an evaporative cooling parameter C is introduced, yielding the following result (Ruffino and di Marzo, 2003):

$$\rho_S c_S V \frac{dT}{dt} = hS(T_G - T) - hSC\beta\sqrt{U} \tag{2}$$

This formulation is based on the assumption that there is little chance of significant water build-up on the link

(Grissom and Wierum, 1981; Paleev and Filippovich, 1966; Berry and Gross, 1972). Considering that the heat transfer coefficient, in the range of Reynolds numbers of concern (i.e. 40–1000), depends on the square root of the velocity (Zukauskas and Ziugzda, 1985), one finds that the activation time is given as:

$$t_A = \frac{RTI}{\sqrt{U}} \ln\left(\frac{T_G - C\beta\sqrt{U} - T_0}{T_G - C\beta\sqrt{U} - T_A}\right) \tag{3}$$

Knowledge of the gas velocity as well as of the water volumetric fraction is needed to evaluate the activation time for secondary sprinklers. It is convenient to relate the evaporative cooling parameter to the sprinkler RTI. Introducing an error of less than 8%, one can obtain the following estimate of the evaporative cooling parameter:

$$C = 1.3RTI^{1/3} \tag{4}$$

Comparison of the activation times obtained experimentally using several hundred commercial sprinklers in various conditions confirm that this model predicts reasonably well the activation time for secondary sprinklers. Figure 1 provides a summary of the measured and calculated activations times for a variety of sprinklers and conditions. Some discrepancies are observed only for bulb-type sprinklers in orientations parallel to the flow because the arm leading into the flow effectively shields the bulb from the water droplets. This results in a reduced evaporative cooling effect. Therefore, for this particular case, the model tends to over estimate the activation time by up to 50%. In the figure, the point represented by the full symbol refers to this situation.

SPRINKLER SPRAY FORMATION

A spray is formed by breaking up a volume of liquid into small drops. This process is referred to as atomization. Atomization facilitates the dispersion of water over a large coverage area for protection of commodities not yet involved in the fire. Furthermore, atomization greatly increases the surface area of the injected volume of water. This increased surface area results in enhanced evaporative cooling of the hot smoke from the fire. Cooling this smoke
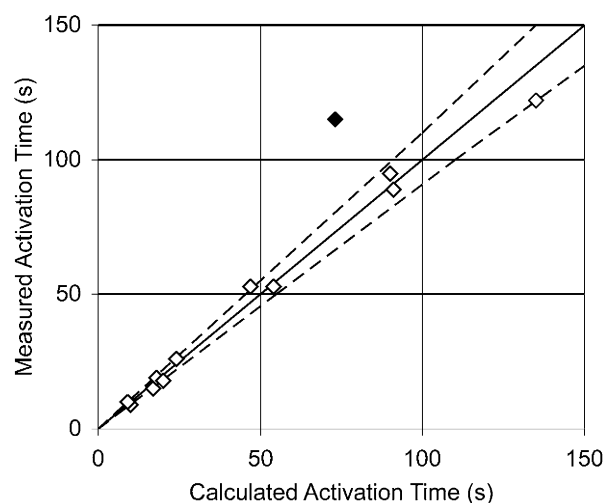
Figure 1. Summary of the measured and calculated activations times for a variety of sprinklers and conditions.

reduces the heat feedback from the fire, resulting in abatement or even extinguishment of the fire.

Atomization Physics

For sprinkler sprays, the atomization consists of three distinct stages, as shown in Figure 2. First, the jet formed at the exit of the injection orifice impinges on a striker plate to form a thin sheet. This thin sheet breaks up more readily than the relatively large-diameter jet formed at the exit orifice. Next, aerodynamic waves are established on the liquid sheet, resulting from the inevitable small disturbances within the flow. These aerodynamic waves are unstable and grow to a critical amplitude which causes the sheet to break into ring-like ligaments. These ligaments are also subject to disturbances and the formation of aerodynamic waves. Finally, the waves on these ligaments grow to a critical amplitude and break the ligaments into small fragments which contract (due to surface tension) to form spherical droplets.

Atomization Modelling

In order to predict spray dispersion, both atomization and drop dispersion (particle tracking) models are needed. Atomization models are required to provide initial conditions for the particle tracking models. The important initial conditions are the initial droplet location, droplet velocity and droplet size. These quantities are readily determined from careful modelling of each stage of the atomization process.

Sheet Formation

Both the velocity and thickness of the liquid sheet are critical parameters that govern the atomization process. The injection configuration of a sprinkler closely resembles that of an impinging jet. Free surface impinging jet theory is used to determine the liquid film thickness and velocity of the thin sheet formed at the deflector of a sprinkler (Watson, 1964). Watson describes the radial spread and boundary layer growth of a liquid jet over a horizontal plane distinguishing four regions of the flow as shown in Figure 2.
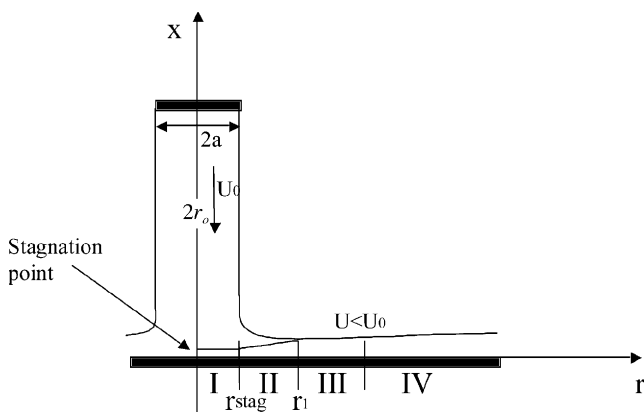
Figure 2. Sprinkler jet forming a viscous film as it impinges against the deflector. Region specific analytical expressions for the film thickness are available.

Region I

This is the stagnation region ($r < d_{jet}/2$). The speed outside the boundary layer rises rapidly from zero at the stagnation point to U_0, the speed with which the jet strikes the plane. The effect of the wall is contained in a very thin boundary layer, which is small compared to the film thickness.

Region II

This is the boundary layer region with Blasius similarity solution. The speed outside the boundary layer is unaffected by this latter and remains almost constant and equal to U_0. In this region, the boundary layer grows until the wall influences the entire thickness of the film.

Region III

This is the transition region. The whole flow is of boundary layer type with velocity profile given by the Blasius solution. The free surface is perturbed by the viscous stresses. The velocity profile changes as r increases; however, the velocity at the free surface remains *nearly* equal to U_0.

Region IV

In this region, the speed of the free surface decays more quickly with r. Velocity profiles in this region can be described by a non-Blasius similarity solution.

Watson's theory provides region specific expressions for the layer thickness based on the radial location. The initial thickness of the sheet is given by the layer thickness at the edge of the deflector. The deflector diameter is thus an important parameter governing the atomization process. For a deflector diameter corresponding to a radial location within region II, the expression for the sheet thickness is given by:

$$h_d = \frac{d_{jet}^2}{8r_d} + 1.659 \times 10^{-2} \left(\frac{7v_L}{U_0} \right)^{1/5} r_d^{4/5} \quad (5)$$

where d_{jet} is the diameter of the jet, r_d is the radius of the deflector plate, U_0 is the initial speed of the jet, and v_L is the liquid kinematic viscosity. It should be noted that r_0 is not the radius of the sprinkler orifice, but the hydraulic radius of the jet and can be calculated from the sprinkler K factor where K is expressed in units of $m^3 \, (s \, Pa^{1/2})^{-1}$. The sheet thickness, h_d, can be rewritten as:

$$h_d = \frac{K}{2\pi r_d} \sqrt{\frac{\rho_L}{2}} + 1.659 \times 10^{-2} \left(\frac{\rho_L}{2P} \right)^{1/10} (7v_L)^{1/5} r_d^{4/5} \quad (6)$$

where ρ_L is the liquid density and P is the total gauge pressure just upstream of the sprinkler. At the deflector plate exit the velocity is radial. The average speed of the sheet at this location may be calculated using the mass conservation between the sprinkler orifice and the deflector plate exit yielding

$$U = \frac{K\sqrt{P}}{2\pi r_d h_d} \quad (7)$$

The speed of the sheet is assumed to be constant and equal to U throughout the breakup process. When the film exits

the striker plate, the thickness of the resulting sheet continues to decrease as it expands radially. The thickness of the sheet is given by

$$h = \frac{r_d h_d}{r} \tag{8}$$

where h is the thickness of the sheet along its radial extent given by the radial location, r. Equations (7) and (8) define important sheet parameters that control the atomization characteristics of the injector.

Sheet Breakup

The central mechanism for atomization is the breakup of the liquid sheet formed by the injector into ligaments (referred to as the sheet → ligament stage in Figure 3). During this stage of the atomization process, disintegration of the continuous liquid stream is initiated. A wave dispersion model is used to predict the growth of the waves that persist on the liquid sheet (Dombrowski and Johns, 1963). In this model, waves are assumed to exist on a thin sheet of liquid surrounded by quiescent gas. A force balance is performed on the undulating sheet considering inertial, pressure, viscous and surface tension forces. After considerable reformulation and simplification, the force balance can be expressed in terms of the growth rate of the waves present on the liquid sheet:

$$\left(\frac{\partial f}{\partial t}\right)^2 + \frac{\mu_L}{\rho_L} n^2 \left(\frac{\partial f}{\partial t}\right) - \frac{2(\rho_A n U^2 - \sigma n^2)}{\rho_L h} = 0 \tag{9}$$

where U is the velocity of the sheet, n is the wavenumber ($n = 2\pi/\lambda$) is the wave number, f is the dimensionless wave amplitude, σ is the surface tension, ρ_A is the gas density, ρ_L is the liquid density, μ_L is the liquid viscosity and h is the sheet thickness. This equation describes the growth rate for a single wavelength having wave number n. Numerous waves of varying wavelengths, and corresponding wave numbers, exist on the liquid sheet; however, only the wave number of the fastest growing wave, $n_{crit,sh}$, is of interest. Both the fastest growing wave, $n_{crit,sh}$, and the corresponding time
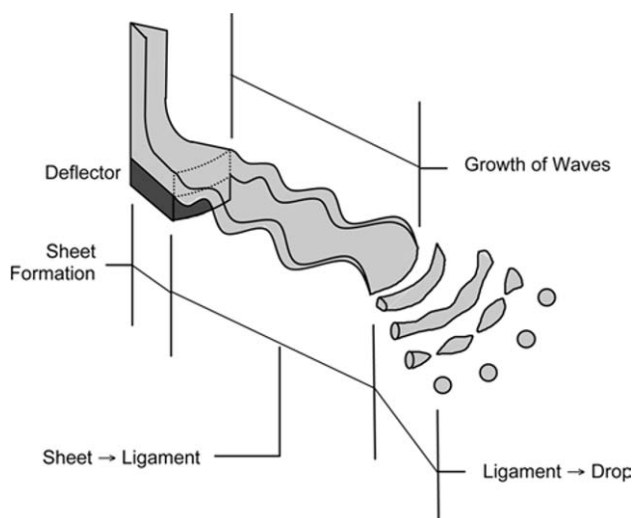
Figure 3. The atomization of the sprinkler jet takes place in three distinct stages. The central mechanism for atomization is critical wave breaking.

varying dimensionless amplitude can be determined by integrating equation (9) with respect to time. Assuming that the sheet velocity, U, will remain constant until breakup, the breakup radius, $r_{bu,sh}$, can be determined from calculating the time taken to reach a critical dimensionless amplitude, $f_{crit,sh}$. This critical amplitude can be determined experimentally and does not depend on operating conditions; however, it may depend on the general injector configuration (Weber, 1931; Dombrowski and Johns, 1964).

The sheet is assumed to breakup into ring-like ligaments having an inner radius equal to the breakup radius, $r_{bu,sh}$, a radial width given by $\lambda_{crit,sh}/2$, and a thickness given by the sheet thickness at breakup, $h_{bu,sh}$. The mass of the ligament, m_{lig}, is thus given by

$$m_{lig} = \pi \rho_L h_{bu,sh}[(r_{bu,sh} + \pi/n_{crit,sh})^2 - r_{bu,sh}^2] \tag{10}$$

An equivalent diameter for the ligament can be determined from

$$m_{lig} = \pi^2 \rho_L \frac{d_{lig}^2}{2}\left(r_{bu} + \frac{d_{lig}}{2}\right) \tag{11}$$

Ligament Breakup

The ligaments formed from the sheet breakup are also unstable and subject to the growth of waves that lead to fragmentation into drops. A simple relationship for the critical wavelength for breakup, $\lambda_{crit,lig}$, is given by (Weber, 1931):

$$\lambda_{crit,lig} = \pi\sqrt{2}d_{lig} \tag{12}$$

This fragment will contract into a droplet. Conserving the mass on the fragment, the characteristic droplet diameter, d_{drop}, is

$$d_{drop}^3 = \frac{3d_{lig}^2 \lambda_{crit,lig}}{2} \tag{13}$$

Weber (1931) also provides an expression for the breakup time:

$$t_{bu,lig} = 12\sqrt{\frac{8\rho_L}{\sigma}}\left(\frac{d_{lig}}{2}\right)^{1.5} \tag{14}$$

The distance that it takes for the ligaments to disintegrate into drops is easily calculated from the relative ligament speed, U, and $t_{bu,lig}$. The initial drop location, r_{drop}, is then given by the total distance the liquid travels until drops are formed:

$$r_{drop} = r_d + U(t_{bu,sh} + t_{bu,lig}) \tag{15}$$

The initial spray velocity, U, initial spray drop size, d_{drop}, and initial spray location, r_{drop}, are completely defined by equations (7), (13) and (15), respectively. These quantities are determined from the sprinkler geometry (K, r_d), injection pressure (P), surrounding flow gas phase fire conditions (ρ_A, μ_A), and liquid properties (σ, ρ_L). It should be noted that for the current formulation the velocity of the gas in the vicinity of the sheet was assumed to be zero; however, the velocity of the fire would increase the relative velocity of the sheet. This relative velocity could replace the sheet velocity in equation (9). These atomization relationships provide a characteristic discrete initial spray conditions for a given
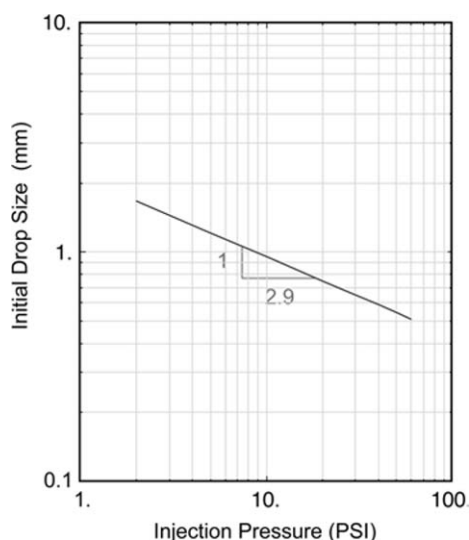
Figure 4. Droplet size predictions of a sprinkler-type spray at standard atmospheric conditions. A simple impinging jet geometry was modelled.

sprinkler geometry and injection pressure, fire condition, and liquid suppressant. Of course in real applications, a multitude of drops with different sizes are created. In order to model this behaviour a stochastic analysis should be introduced (Rizk and Mongia, 1991). Only the discrete equations have been provided in this paper to illustrate the physics of the atomization process.

Results from the atomization model are presented in Figures 4 and 5 to provide some sprinkler spray characteristics and to demonstrate the sensitivity of the models to injection pressure and ambient temperature. These predictions were obtained for a sprinkler type spray using an impinging jet atomization configuration. The atomization model predicts a strong dependence of drop size on injection pressure. Figure 4 shows that the droplet diameter,

$d_{drop} \approx P^{-1/3}$. The initial drop size and location are also very sensitive to the gas phase environmental temperature as shown in Figure 5. The increased gas temperature reduces the gas density, ρ_A in equation (9), which results in slower wave growth rates and longer sheet breakup times. Experiments are currently being conducted to compare and validate these model predictions.

SPRAY DISPERSION

The spray dynamics are strongly coupled with the continuous phase dynamics; therefore, equations for both phases should be solved simultaneously to obtain accurate solutions of the spray dispersion. The conservation equations of mass, momentum, and energy are typically solved using an Eulerian formulation for the continuous phase while the conservation equations are normally solved using a Lagrangian formulation for the dispersed phase. The governing equations for the continuous phase are the well-known equations of continuum mechanics and therefore will not be included in this discussion. It should be noted that the source terms in the gas phase mass, momentum and energy equations are determined from the conservation equations for drops. The equations describing drop dynamics can be determined from mass, momentum, and energy balances on the droplet assuming uniform properties (Crowe *et al.*, 1997). These equations are integrated using a time marching approach starting from specified initial conditions. The Lagrangian formulation of the dispersed phase is very sensitive to these initial conditions and reliable estimates for the initial droplet characteristics are required for accurate dispersion predictions. The initial conditions for the drop dispersion equations are provided by the atomization model previously discussed.
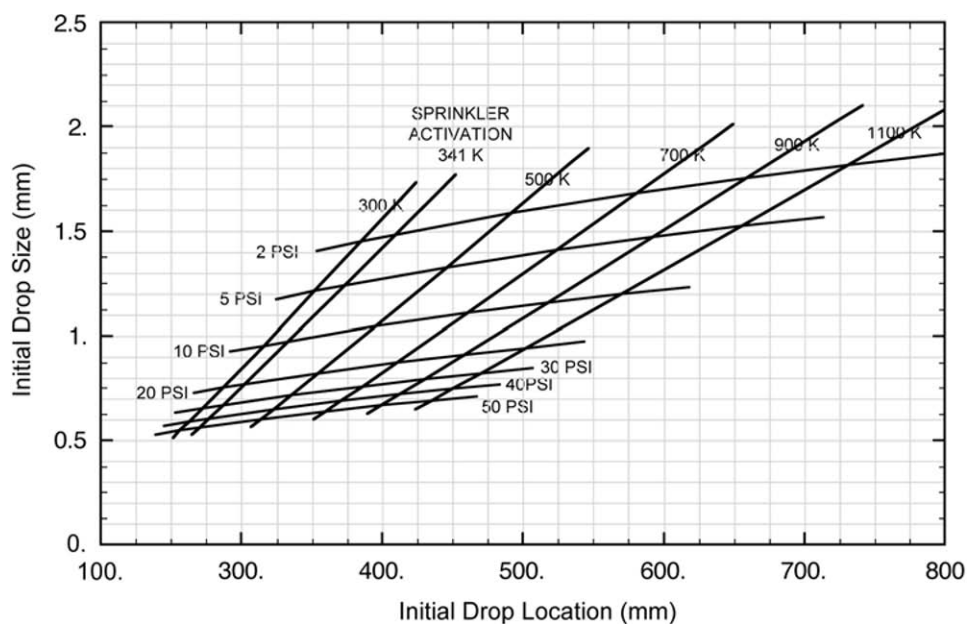
Figure 5. Predicted initial drop conditions of a sprinkler-type spray as a function of injection pressure and elevated ambient temperature. A simple impinging jet geometry was modelled.

The acceleration of the droplet is described by the momentum conservation equation:

$$\frac{d\vec{u}_d}{dt} = \frac{f}{\tau_v}(\vec{u} - \vec{u}_{drop}) + \vec{g} \qquad (16)$$

where f_{drag} is the friction factor describing the ratio of the drag coefficient to Stokes drag given by $f_{drag} = (1 + 0.15Re_r^{0.687})$ (Schiller and Naumann, 1933), τ_v is a velocity response time given by $\tau_v = \rho_l d_{drop}^2/18\mu_A$, $\vec{u}$ is the gas velocity, $\vec{u}_{drop}$ is the drop velocity, and $\vec{g}$ is the gravitational acceleration vector, Re_r is the Reynolds number based on the relative velocity, ρ_L is the liquid density, d_{drop} is the drop diameter, and μ_A is the gas viscosity. The evaporation of the droplet is described by the mass conservation equation:

$$\frac{dm_{drop}}{dt} = Sh\pi d_{drop}\rho_l D_v(\omega_{H_2O,\infty} - \omega_{H_2O,s}) \qquad (17)$$

where the Sherwood number is $Sh = h_m d_{drop}/D_v$, h_m is the convective mass transfer coefficient, D_v is the mass diffusivity, $\omega_{H_2O,\infty}$ is the mass fraction of water vapour in the gas environment, and $\omega_{H_2O,s}$ is the mass fraction of water vapour at the droplet surface. The heating of the droplet is described by the energy conservation equation:

$$\frac{dT_{drop}}{dt} = \frac{d_{drop}}{2k_A}\frac{1}{\tau_T}(\alpha_{rad}G - \varepsilon\sigma_{rad}T_{drop}^4)$$
$$+ \frac{Nu}{2}\frac{1}{\tau_T}(T_\infty - T_{drop})$$
$$+ \frac{Sh}{2}\frac{1}{\tau_T}\frac{Pr}{Sc}\frac{h_L}{c_A}(\omega_{H_2O,\infty} - \omega_{H_2O,s}) \qquad (18)$$

where T_d is the droplet temperature, α_{rad} is the radiative absorbtivity of the droplet, G is the irradiation, ε is the radiative emissivity, σ_{rad} is the Stefan–Boltzmann constant, k_a is the thermal conductivity of the gas, $\tau_T = c_l\rho_l d_{drop}^2/12k_A$ is a characteristic heating time for the droplet, c_l is the specific heat of the liquid, the Nusselt number is given by $Nu = h_T d_{drop}/k_A$, where h_T is the convective heat transfer coefficient, the Prandtl number is given by $Pr = v_A/\alpha_A$, the Schmidt number is given by $Sc = v_A/D_v$, T_∞ is the gas temperature, h_L is the latent heat of vapourization, and c_A is the specific heat of the gas.

SPRAY SURFACE COOLING

Once the water droplets reach solid surfaces exposed to the thermal radiation from the fire and to the hot gases convective heat transfer, they provide evaporative cooling thus reducing the average surface temperature. By keeping the surface temperature low, pyrolysis of the solid materials is curtailed and the solid is protected. The fire is contained since no more fuel becomes available and suppression is achieved.

To characterize these phenomena, the average surface temperature must be evaluated under convective and radiant heat input while a sparse water spray is applied. The vapourization of single droplets deposited on solid surfaces has been studies extensively. Two representative references are Bonacina *et al.* (1979) and Makino and Michiyoshi (1984). A complete representation of the liquid–solid transient thermal interactions is given by di Marzo *et al.* (1993).

The solid is treated with a boundary element technique yielding the following relationship for surface temperatures:

$$T(r, t) - T_0(r)$$
$$= \int_0^t \int_0^\infty \nabla[T(r^*, t^*) - T_0(r^*)]r^* t^{*-3/2}$$
$$\times L_0\left(\frac{2rr^*}{4\alpha t^*}\right)\exp\left[-(r - r^*)^2/(4\alpha t^*)\right]dr^*\,dt^* \qquad (19)$$

The temperature gradient at the surface, shown inside the integrals, is given by the solution of the thermal transient in the liquid subjected to a liquid–vapour boundary condition that encompasses water vapour mass transfer as well as the convective heat transfer component (White *et al.*, 1994). This boundary condition can be expressed as:

$$k_L\nabla T(r, t)$$
$$= 0.62\left(\frac{h_T\Lambda}{c_A Le^{2/3}}\right)\frac{x - x_\infty}{1 - x} + h_T[T_i(r, t) - T_\infty]$$
$$= AT_i(r, t) - B \qquad (20)$$

The radiant heat is absorbed in the bulk of the liquid. Consider a steady-state situation where the rate of change of the internal energy of the liquid is small. In this case one can integrated the energy equation for the liquid subjected to the above-mentioned boundary condition and equating the liquid and solid temperature at that interface. In order to simplify the formulation, it is useful to linearize equation (20) expressing the molar fractions in terms of the temperature making use of the Clausius–Clapeyron relationship. The radiant volumetric heat deposit in the liquid layer is expressed as H to yield:

$$-k\nabla T(r, t) = \frac{k_L}{1 - A\delta}\left[\frac{AH\delta^2}{2k_L} - H\delta - AT(r, t) - B\right] \qquad (21)$$

With this model, one can obtain the time of vapourization associated with droplets of a given size on solid surfaces at a given initial temperature. To model a full water spray, close form solutions are introduced to represent the solid surface temperature during and after a single droplet vapourization transient. These solutions are based on Carslaw and Jaeger (1959) and can be represented as:

$$T_0 - T(r, t) = \frac{qR}{k}\int_0^\infty J_0(rr^*)J_1(Rr^*)\text{erf}(r^*\sqrt{\alpha t})\frac{dr^*}{r^*}$$
$$T_0 - T(r, t) = \frac{qR}{k}\int_0^\infty J_0(rr^*)J_1(Rr^*)\{\text{erf}(r^*\sqrt{\alpha t})$$
$$- \text{erf}[r^*\sqrt{\alpha(t - \tau)}]\}\frac{dr^*}{r^*} \qquad (22)$$

These equations describe the surface temperature evolution near the droplet site. In the far field a simpler representation is achieved considering the droplet as a point sink. This is expressed in the following form:

$$T_0 - T(r, t) = \frac{qR^2\tau}{4\alpha(t - 0.6\tau)^{3/2}\sqrt{\pi\rho ck}}\exp\left[\frac{-r^2}{4\alpha(t - 0.6\tau)}\right] \qquad (23)$$
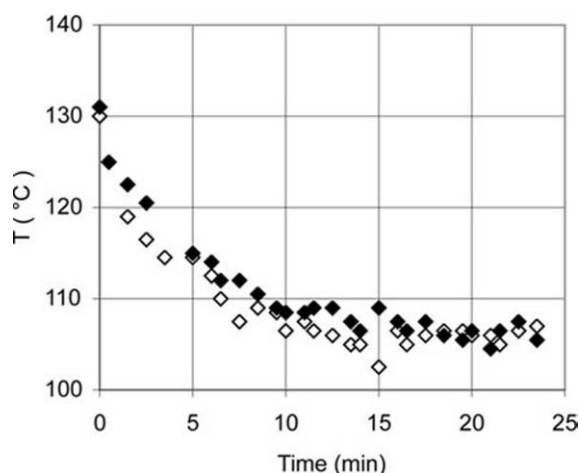
Figure 6. Average surface temperature transient: $T_0 = 131°C$; $G = 0.50\,\mathrm{g\,m^{-2}\,s^{-1}}$ (the open symbols represent the experimental data and the closed ones represent the spray model computations; di Marzo and Tinker, 1996).

In the previous three equations the solid–liquid boundary condition is approximated with a constant heat flux condition expressed in terms of the droplet volume and of the initial wetted radius as the droplet impacts the solid surface as:

$$q = \frac{\rho_L V_D \Lambda}{\pi R^2} \qquad (24)$$

By keeping an appropriate inventory of the droplets reaching the solid surface, the temperature of the solid surface is determined by superposing all these cooling effects and the space and time averaged surface temperature can be calculated. Figure 6 shows how the model predictions match the experimental results for an initial solid surface temperature of 131°C and a water mass flux of $0.50\,\mathrm{g\,m^{-2}\,s^{-1}}$.

SUMMARY

The important physical processes affecting sprinkler performance have been identified as activation, atomization, dispersion and droplet surface cooling. These processes have been described and discussed with mathematical models, model predictions, and experimental results. These mathematical models can be used for predicting primary and secondary sprinkler activation times. A model describing cooling effects from adjacent sprinklers resulting in delayed secondary sprinkler activation time has been recently developed and provided herein. Atomization models and droplet tracking models developed for sprinklers can provide very detailed information characterizing the initial spray and its subsequent dispersion. The atomization models recently developed for sprinklers show a strong dependence of the initial droplet conditions on not only injection pressure, but also on environmental fire conditions. Finally, detailed analysis has been conducted to describe the interaction of the drops with hot surfaces to predict the cooling and suppression behaviour of the fire. These models are critical for developing an understanding of suppression behaviour in fires and can be used to predict the performance and behaviour of fire suppression systems for development, design, or analysis applications.

NOMENCLATURE

A, B	constants, see equation (20)
c	specific heat of the solid
c_A	specific heat of the air
c_L	specific heat of the liquid
c_S	specific heat of the sensor
C	evaporative cooling parameter, see equation (4)
d	diameter
D_v	mass diffusivity of water vapour
erf	error function
f	dimensionless wave amplitude
f_{drag}	friction factor
$\vec{g}$	gravitational acceleration vector
G	irradiation onto droplet surface
h	sheet thickness
h_M	convective mass transfer coefficient
h_T	convective heat transfer coefficient
h_d	thickness of sheet at deflector exit
H	radiant volumetric heat deposited in the liquid layer
I_0, J_0, J_1	Bessel's functions
k	thermal conductivity of the solid
k_A	thermal conductivity of the air
k_L	thermal conductivity of the water
L_0	modified Bessel's function $e^{-r^*} I_0(r^*)$
Le	Lewis number
M	mass
n	wave number
Nu	Nusselt number
P	sprinkler injection total gauge pressure
Pr	Prandtl number
q	heat flux at the solid surface
r	radial coordinate
r_d	radial dimension of deflector
r^*, t^*	dummy variables of integration, see equations (19) and (22)
R	droplet radius after impact on the surface
Re_r	Reynolds number based on the droplet relative velocity
RTI	response time index, see equation (1)
S	sensor surface area
Sc	Schmidt number
Sh	Sherwood number
t	time
t_A	time of activation for the sprinkler
T	temperature
T_0	initial temperature
T_A	temperature of activation for the sprinkler
T_G	gas temperature
T_i	solid–liquid interfacial temperature
T_∞	ambient temperature
$\vec{u}$	gas velocity
U	velocity
U_0	sheet velocity
V	volume of the sensor
V_D	droplet volume
x	molar fraction
x_∞	molar fraction in the far field

Greek symbols

α	thermal diffusivity
α_{rad}	droplet radiative absorptivity
β	water droplets volumetric fraction
δ	droplet thickness
ε	droplet emissivity
λ	wavelength
Λ	latent heat of vapourization
μ_L	viscosity of the liquid
ν_L	kinematic viscosity of the liquid
ρ	density of the solid
ρ_L	density of the liquid
ρ_S	density of the sensor
ρ_A	gas density
σ	liquid surface tension
σ_{rad}	Stefan–Boltzmann constant
τ	droplet vapourization time
τ_V	characteristic drop velocity response time
τ_T	characteristic drop temperature response time
∇T	temperature gradient at the solid surface within the solid

$\omega_{H_2O,s}$	mass fraction of water vapour at the droplet surface
$\omega_{H_2O,s}$	mass fraction of water vapour in the gas environment

Subscripts

bu	breakup
crit	critical
drop	drop
jet	jet
lig	ligament
sh	sheet

REFERENCES

Aihara, T. and Fu, W.S., 1986, Effect of droplets-size distribution and gas-phase flow separation upon inertia collecting droplets by bluff-bodies in gas-liquid mist flow, *Int J Heat Mass Transfer*, 12: 389–403.

Berry, M.R. Jr. and Gross, W.P., 1972, An integral analysis of condensing annular-mist flow, *AIChE J*, 18: 754–761.

Bonacina, C., Del Giudice, S. and Comini, C., 1979, Dropwise evaporation, *Trans ASME, J Heat Transfer*, 101: 441–446.

Carslaw, H.S. and Jaeger, J.C., 1959, *Conduction of Heat in Solids* (Clarendon Press, Oxford) pp 87–88, 214–216 and 264.

Crowe, C., Sommerfeld, M. and Tsuji, Y., 1997, *Multiphase Flows with Droplets and Particles* (CRC Press, New York) pp 57–107.

di Marzo, M. and Tinker, S., 1996, Evaporative cooling due to a sparse spray, *Fire Safety J*, 27: 289–303.

di Marzo, M., Tartarini, P., Liao, Y., Evans, D. and Baum, H., 1993, Evaporative cooling due to a gently deposited droplet, *Int J Heat Mass Transfer*, 36: 4133–4139.

Dombrowski, N. and Johns, W.R., 1963, The aerodynamic instability and disintegration of viscous liquid sheets, *Chem Eng Sci*, 18: 203–214.

Grant, G., Brenton, J. and Drysdale, J., 2000, Fire suppression by water sprays, *Prog Energy Combus Sci*, 26: 79–130.

Grissom, W.M. and Wierum, F.A., 1981, Liquid spray cooling of a heated surface, *Int J Heat Mass Transfer*, 24: 261–271.

Heskestad, G. and Bill, R.G., 1988, Modeling of thermal responsiveness of automatic sprinklers, *Fire Safety Science* (Hemisphere, New York), pp 603–612.

Makino, K. and Michiyoshi, I., 1984, The behavior of a water droplet on heated surfaces, *Int J Heat Mass Transfer*, 27: 781–791.

Novozhilov, V., 2001, Computational fluid dynamics modeling of compartment fires, *Prog Energy Combust Sci*, 27: 611–666.

Paleev, I.I. and Filippovich, B.S., 1966, Phenomena of liquid transfer in two-phase dispersed annular flow, *Int J Heat Mass Transfer*, 9: 1089–1093.

Rizk, N.K. and Mongia, H.C., 1991, Model for airblast atomization, *J Propul*, 7: 305–311.

Ruffino, P. and di Marzo, M., 2003, Temperature and volumetric fraction measurements in a hot gas laden with water droplets, *Trans ASME J Heat Transfer*, 125: 356–364.

Schiller, L. and Naumann, A.Z., 1933, *Z Ver Dtsch Ing*, 77: 318–320.

Watson, E.J., 1964, The radial spread of a liquid jet over a horizontal plane, *J Fluid Mech*, 20: 481–499.

Weber, Z., 1931, *Angew Math Mech*, 11: 136–154.

White, G., Tinker, S. and di Marzo, M., 1994, Modeling of dropwise evaporative cooling on a semi-infinite solid subjected to radiant heat, in *Fire Safety Science* (International Association of Fire Safety Science), pp 217–228.

Zukauskas, A. and Ziugzda, J., 1985, *Heat Transfer of a Cylinder in Crossflow* (Hemisphere, New York), pp 138–140.